



King's Research Portal

DOI:

[10.1007/s00018-019-03263-6](https://doi.org/10.1007/s00018-019-03263-6)

Document Version

Peer reviewed version

[Link to publication record in King's Research Portal](#)

Citation for published version (APA):

Zhao, T., Wu, K., Hogstrand, C., Xu, Y. H., Chen, G. H., Wei, C. C., & Luo, Z. (2020). Lipophagy mediated carbohydrate-induced changes of lipid metabolism via oxidative stress, endoplasmic reticulum (ER) stress and ChREBP/PPAR pathways. *Cellular and Molecular Life Sciences*, 77, 1987–2003.
<https://doi.org/10.1007/s00018-019-03263-6>

Citing this paper

Please note that where the full-text provided on King's Research Portal is the Author Accepted Manuscript or Post-Print version this may differ from the final Published version. If citing, it is advised that you check and use the publisher's definitive version for pagination, volume/issue, and date of publication details. And where the final published version is provided on the Research Portal, if citing you are again advised to check the publisher's website for any subsequent corrections.

General rights

Copyright and moral rights for the publications made accessible in the Research Portal are retained by the authors and/or other copyright owners and it is a condition of accessing publications that users recognize and abide by the legal requirements associated with these rights.

- Users may download and print one copy of any publication from the Research Portal for the purpose of private study or research.
- You may not further distribute the material or use it for any profit-making activity or commercial gain
- You may freely distribute the URL identifying the publication in the Research Portal

Take down policy

If you believe that this document breaches copyright please contact librarypure@kcl.ac.uk providing details, and we will remove access to the work immediately and investigate your claim.

[Click here to view linked References](#)

Lipophagy mediated carbohydrate-induced changes of lipid metabolism via oxidative stress, endoplasmic reticulum (ER) stress and ChREBP/PPAR γ pathways

Tao Zhao¹, Kun Wu¹, Christer Hogstrand³, Yi-Huan Xu¹, Guang-Hui Chen¹, Chuan-Chuan Wei¹, Zhi Luo^{1,2,*}

¹ Key Laboratory of Freshwater Animal Breeding, Ministry of Agriculture, Fishery College, Huazhong Agricultural University, Wuhan 430070, China

² Laboratory for Marine Fisheries Science and Food Production Processes, Qingdao National Laboratory for Marine Science and Technology, Qingdao 266237, China

³ Diabetes and Nutritional Sciences Division, School of Medicine, King's College London, United Kingdom

*Corresponding author. Prof. Zhi Luo, Tel.: +86-27-8728-2113; Fax: +86-27-8728-2114; Email address: luozhi99@mail.hzau.edu.cn; luozhi99@aliyun.com (Z. Luo).

Abstract:

High carbohydrate diets (HCD) can induce the occurrence of nonalcoholic fatty liver disease (NAFLD), characterized by dramatic accumulation of hepatic lipid droplets (LDs). However, the potential molecular mechanisms are still largely unknown. In this study, we investigated the role of autophagy in the process of HCD-induced changes of hepatic lipid metabolism, and to examine the process of underlying mechanisms during these molecular contexts. We found that HCD significantly increased hepatic lipid accumulation and activated autophagy. Using primary hepatocytes, we found that HG increased lipid accumulation and stimulated the release of NEFA by autophagy-mediated lipophagy, and that lipophagy significantly alleviated high glucose (HG)-induced lipid accumulation. Oxidative and endoplasmic reticulum (ER) stress pathways played crucial regulatory roles in HG-induced lipophagy activation and HG-induced changes of lipid metabolism. Further investigation found that HG-activated lipophagy and HG-induced changes of lipid metabolism were via enhancing carbohydrate response element binding protein (ChREBP) DNA binding capacity at PPAR γ promoter region, which in turn induced transcriptional activation of the key genes related to lipogenesis and autophagy. The

present study, for the first time, revealed the novel mechanism for lipophagy mediating HCD-induced **changes of lipid metabolism** by oxidative stress and ER stress, and ChREBP/ PPAR γ pathways. Our study provided innovative evidence for the direct relationship between carbohydrate and lipid metabolism via ChREBP/ PPAR γ pathway.

Keywords: Dietary carbohydrate; Lipid deposition; Lipid metabolism; Regulatory pathways; Lipophagy

Abbreviations: 3-MA, 3-methyl adenine; 4-PBA, 4-Phenylbutyric acid; 6PGD, 6-phosphogluconate dehydrogenase; ACCa, acetyl-CoA carboxylase a; ACSL, acyl-CoA synthetase long-chain; AO, acridine orange; ATF, activating transcription factor; ATG, autophagy related gene; BSA, bovine serum albumin; CF, condition factor; ChREBP, carbohydrate response element-binding protein; CPT-1, carnitine palmitoyltransferase-1; CQ, chloroquine; DCFH2-DA, 2', 7'-dichlorodihydrofluorescein diacetate; eIF2 α , eukaryotic translation initiation factor 2 α ; ERS, endoplasmic reticulum stress; FABPL, fatty acid-binding protein liver; FAS, fatty acid synthase; FBW, final mean body weight; FCR, feed conversion rate; FFA, free fatty acids; FI, feed intake; G6PD, glucose 6-phosphate dehydrogenase; GLUT, glucose transporter; GRP78, Glucose-regulated protein 78; GSH, glutathione; GSSG, glutathione disulfide; HCD, high carbohydrate diet; H&E, hematoxylin and eosin; HG, high glucose; HSI, hepatosomatic index; HSL, hormone-sensitive lipase; ICD, intermediate carbohydrate diet; ICDH, isocitrate dehydrogenase; IRE1 α , inositol requiring 1 α ; LCD, low carbohydrate diet; LD, lipid droplet; LXR a, liver x receptor a; MAP1LC3B, microtubule-associated proteins 1A/1B light chain 3B; IBW, initial mean body weight; M199, medium-199; MDA, malondialdehyde; MDC, monodansylcadaverine; ME, malic enzyme; NAC, N-acetyl-L-cysteine; NAFLD, nonalcoholic fatty liver disease; NEFA, nonesterified fatty acid; OD, optical density; ORO, oil red O; PERK, protein kinase R (PKR)-like ER kinase; PPAR, peroxisome proliferator-activated receptor; PVDF, polyvinylidene difluoride; ROS, reactive oxygen species; S.E.M, standard error of the mean; SGR, specific growth rate; SOD, superoxide dismutase; SREBP-1, sterol regulatory element binding proteins-1; TG, triglyceride; UPR, unfolded protein response; VAI, visceral adipose index; VSI, viscerosomatic index; WG, weight gain; XBP1, x-box binding protein 1.

Introduction

Non-alcoholic fatty liver disease (NAFLD), characterized by the excessive triglyceride (TG) accumulation in the livers, has been increasing in recent years [1]. The spectrum of NAFLD ranges from simple fatty liver to nonalcoholic steatohepatitis (NASH), which may result in liver fibrosis and eventually the development of hepatocellular carcinoma [2]. At present, treatment approaches are limited because of the unclear pathological mechanism of NAFLD. It is well known that the diet rich in carbohydrate along with other factors can induce hepatic NAFLD and NASH [3, 4]. However, the additional mechanisms of dietary carbohydrate leading to the NAFLD are not fully elucidated.

Autophagy is a highly conserved self-renewal process in eukaryotic cells, characterized by the engulfment of cytoplasmic materials into double-membrane vesicles (autophagosomes) for subsequent degradation in lysosomes [5]. Studies suggested that autophagy regulates lipid metabolism by eliminating TG and its activation plays a key inhibitory role in the development of NAFLD [6]. Moreover, lipophagy, one kind of autophagy, regulates lipid metabolism by breaking lipid droplets down and enhancing the rate of mitochondrial β -oxidation [6-8]. Impaired lipophagy will increase cellular lipid storage and result in the occurrence of NAFLD [9, 10].

Several signaling pathways were reported to regulate the autophagic process, such as oxidative stress, endoplasmic reticulum (ER) stress and PPAR γ pathways. Oxidative stress, which results from an imbalance between free radical production and scavenging, induces the formation of autophagy [11]. Oxidative stress also accelerates lipid accumulation by disrupting mitochondrial functions and reducing oxidation of fatty acids [12-14]. The ER is the intracellular important organelle for the synthesis and folding of proteins. ER stress will occur if ER homeostasis is disrupted and unfolded /unprocessed proteins are accumulated within the ER. Increasing evidences demonstrated that ER stress might be associated with autophagy [15, 16], and involved in the development of NAFLD [17, 18]. The PPAR γ is the important transcriptional factor which regulates autophagic process and lipid metabolism [19, 20].

Thus, in view of the important role of autophagy in regulating lipid metabolism, and the relevant signaling pathways can activate autophagy, we hypothesis that these

molecular events mediated high carbohydrate diets-induced changes of lipid accumulation in the liver. If our hypothesis can be confirmed, our results will provide insight into key pathological mechanisms contributing towards fatty liver occurrence.

Fish are the largest group of vertebrates in the world. During the evolution, fish were considered to experience the fish-specific genome duplication event (FSGD) [21]. By analyzing whole-genome sequence information, Gong et al. [22] found the FSGD in yellow catfish *Pelteobagrus fulvidraco*, an important freshwater omnivorous fish in China and other countries [23]. Some duplicated genes evolve new functions that in turn result in novel regulatory mechanism [21]. Therefore, using yellow catfish as a model, we hope to find some novel regulatory mechanism of metabolism. Moreover, previous study in our laboratory pointed that high dietary carbohydrate increased liver lipid deposition and developed fatty liver symptom in juvenile yellow catfish [23]. Accordingly, the present study investigated the mechanism of dietary carbohydrate influencing lipid metabolism and dissected the roles of lipophagy mediating carbohydrate-induced changes of lipid metabolism via oxidative stress, ER stress and ChREBP/PPAR γ pathways.

Materials and Methods

Animals feeding and sampling

The protocols of all animal and cells experiments were approved by the ethical guidelines of Huazhong Agricultural University for the care and use of laboratory animals. The experimental protocols were similar to those in our recent study [24], as described in Yang et al. [25]. Briefly, 270 uniformly-sized yellow catfish (4.1 ± 0.01 g, mean \pm SEM) were randomly stocked in 9 circular fiberglass tanks, 30 fish for each tank. They were fed with three experimental diets with dietary carbohydrate levels at 17.2% (low carbohydrate diet, LCD), 22.8% (intermediate carbohydrate diet, ICD) and 30.2% (high carbohydrate diet, HCD), respectively, and corn starch was used as the carbohydrate source (Supplementary Table 1). Each diet was assigned to 3 tanks in a completely randomized manner and fed to apparent satiation twice daily at 8:00 am and 4:00 pm for 10 weeks. During the experiment, water temperature ranged from 25.7°C to 28.6°C; dissolved oxygen and NH $_4$ -N were 6.07 ± 0.01 mg/L and 0.11 ± 0.01 mg/L, respectively.

At the end of the 10-week feeding trial, all fish were fasted for 24h before sampling. Fish were anesthetized with MS-222 (100 mg/L water), and then, counted and weighed to determine survival, WG (weight gain) and SGR (specific growth rate).

After obtaining the final total weight of fish in each tank, ten fish per tank were randomly collected, weighed and dissected on ice to obtain the liver and viscera samples for the calculation of VSI (viscerosomatic index), VAI (visceral adipose index), and HSI (hepatosomatic index). Another six fish were randomly selected from per tank, and the liver and blood were immediately collected. The livers were quickly frozen in liquid nitrogen and stored at -80°C for RNA and protein isolation. The blood was centrifuged at 3500 g min⁻¹ for 10 mins, and then serum was separated to determine glucose content. Another three fish per tank were randomly selected and the liver were collected, and then fixed in 10% neutral buffered formalin and 2.5% paraformaldehyde for histological, histochemical and ultrastructural observation, respectively. For analyzing hepatic enzyme activity and TG content, another six fish per tank were randomly selected and the liver were collected, and then were immediately frozen in liquid nitrogen and stored at -80°C for subsequent analysis.

Cell culture and treatments

Primary hepatocytes were isolated from *P. fulvidraco* liver and cultured as described previously [24]. In order to determine the mechanism of autophagy influencing the glucose-induced lipid deposition, we used the pharmacological autophagy-lysosomal pathway inhibitor 3-MA (S2767; Selleck Chemicals, Houston, TX, USA) or CQ (C6628; Millipore Sigma, Burlington, MA, USA), respectively, to incubate the hepatocytes. To illuminate the mechanism by which glucose induced autophagy and lipid accumulation, the corresponding inhibitors of the signaling pathways were used, including 4-PBA (ER stress inhibitor, SML0309; MilliporeSigma), NAC (ROS scavenger, S1623; Selleck Chemicals) and T0070907 (PPAR γ inhibitor, S2871; Selleck Chemicals). The concentrations and incubation time for all experiments are reported in the Figure legends.

MTT assay for cell viability

The protocols for MTT assay was based on these described in our recent publication [26].

Histological, histochemical analysis, transmission electron microscopy (TEM) observation and Bodipy 493/503 staining

Hematoxylin-eosin (H&E staining), histochemical (Oil Red O staining) and Bodipy 493/503 (D3922; Thermo Fisher Scientific Waltham, MA, USA) staining for livers and hepatocytes were conducted according to the methods as our previously described [14, 24]. For statistics of relative areas for hepatic vacuoles in H&E and

lipid droplets in oil-red O staining, we randomly examined 10 fields and each sample were quantified with Image J. The protocols for TEM observation have been described in Wei et al. [24]. For the Bodipy 493/503 staining, hepatocytes were observed with a laser scanning confocal microscope (Leica Microsystems, Wetzlar, Germany) to visualize the intensity of fluorescence. In those microscopes, scale bar was 10 μ m with $\times 40$ objective and $\times 3$ zoom, and scale bar was 5 μ m with $\times 40$ objective and $\times 6$ zoom, respectively. The green dots were defined as lipid droplet, which were quantified by Image-Pro Plus 6.0 (Media Cybernetics, Silver Spring, MD, USA).

Determination of the contents of TG, nonesterified fatty acid (NEFA) and serum glucose

TG, NEFA and serum glucose concentrations were determined with commercial kits (Nanjing Jiancheng Bioengineering Institute, Nanjing, China), according to the manufacturer's instructions. Proteins concentrations were determined with the Bradford Protein Assay Kit of Nanjing Jiancheng Bioengineering Institute (Nanjing, China).

Determination of enzymatic activities and indices of oxidative stress

Activities of several enzymes related to lipid metabolism, such as G6PD (glucose 6-phosphate dehydrogenase), 6PGD (6-phosphogluconate dehydrogenase), ME (malic enzyme), ICDH (isocitrate dehydrogenase), FAS (fatty acid synthase), and CPT I (carnitine palmitoyltransferase 1), were measured as previously described [24, 26]. One unit of enzyme activity, defined as the amount of enzyme that converts 1 μ M of substrate to product per minute at 30°C, was expressed as units per milligram of soluble protein. Protein concentrations were determined with the Bradford Protein Assay Kit (Nanjing, China).

We also measured several parameters involved in oxidative stress, such as SOD activity and the levels of MDA, ROS, GSH and GSSG. SOD activity was measured based on aerobic reduction of NBT at 535nm by superoxide radicals following the method described in Pan et al. [14]. MDA level was measured using malondialdehyde (MDA) assay kit from Nanjing Jiancheng Bioengineering Institute (Nanjing, China) base on measuring thiobarbituric acid-malondialdehyde (TBA-MDA) complex absorbance at 532nm. Intracellular ROS level was measured using oxidation-sensitive fluorescent probe DCFH-DA (287810; MilliporeSigma) as described previously [26]. Liver and intracellular GSH and GSSG levels were determined according to the

studies by Giustarini et al. [27]. All these analyses were conducted in three replicates.

Detection of autophagic vesicles and free Ca²⁺ in the hepatocytes

Detection of autophagic vesicles and free Ca²⁺ in the hepatocytes were performed according to recent studies [24, 28, 29]. Fluo-4 AM (F14201; Thermo Fisher Scientific) was used to detect free Ca²⁺. AO (318337; MilliporeSigma), MDC (30432; MilliporeSigma) were used to detect the autophagic vesicles and Lyso-Tracker Red DND-99(L7528; Thermo Fisher Scientific) was used to detect lysosomal activity based on the published protocols [28]. Briefly, the treated cells were incubated with the corresponding reagents for 30 min, followed by 3 PBS washes, and then observed with the laser scanning confocal microscope (Leica) to visualize the intensity of fluorescence (×40 objective and ×2 zoom, scale bar: 25µm). The fluorescences of the stained cells were quantified on a CytoFlex Flow Cytometer (Beckman Coulter) and data analysis was performed with FlowJo v.10 software. The relative fluorescence intensity of Ca²⁺, and co-localization of lipid droplets and autolysosomes were quantified using Image J analysis software.

RNA isolation and quantitative real-time PCR (qRT-PCR)

Total RNA was isolated with Trizol reagent (Thermo Fisher Scientific) and transcribed into the cDNA with a Reverse Transcription Kit (Thermo Fisher Scientific). qPCR assays were performed based on the methods described in our recent publications [26]. The gene specific primers are given in [Supplementary Table 2](#). Ten housekeeping genes (18S rRNA, β-actin, HPRT, B2M, UBCE, TUBA, GAPDH, RPL7, TBP and ELFA) were selected to test their transcription stability. The relative expression of genes was calculated using the 2^{-ΔΔCt} method when normalizing to the geometric mean of the best combination of 2 genes as analyzed by geNorm (<https://genorm.cmgg.be/>).

Western blotting

Based on the protocol described in our recent publication [24], we used western blot analysis to test protein expression levels, such as LC-3B, Beclin-1, SQSTM1/p62, BiP/GRP78 and PPARγ. Briefly, liver and cell lysates were prepared with RIPA buffer (Thermo Fisher Scientific). Proteins (40µg from each sample) were then separated on 10 or 15% SDS-polyacrylamide gel (depending on the molecular size of proteins to be analyzed), transferred to PVDF membranes (Thermo Fisher Scientific), and then blocked with 8% (w/v) skimmed milk in TBST buffer (20 mM Tris-HCl, pH 7.5, 150 mM sodium chloride, 0.1% Tween 20) for 1 h and then washed thrice with TBST

buffer for 10 min each, followed by incubation with specific primary antibodies including rabbit anti-LC3B (1:1000, ab51520; Abcam, Cambridge, MA, USA), anti-Beclin-1 (1:1000, #3738; Cell Signaling Technology, Danvers, MA, USA), anti-SQSTM1/p62 (1:500, #5114; Cell Signaling Technology), anti-BiP/GRP78 (1:500, #3183; Cell Signaling Technology), anti-PPAR γ (1:500, ab59256; Abcam), anti-GAPDH (1:4000, #2118; Cell Signaling Technology), and anti- β -actin(1:2000, #4970; Cell Signaling Technology) for overnight at 4°C, followed by incubating with goat anti-rabbit IRDye 800CW secondary antibody (1:20000, 926-32211; Li-Cor Biosciences, Lincoln, NE, USA) or HRP-conjugated anti-rabbit IgG antibody (1:2000, #7074; Cell Signaling Technology). Immunoreactive bands were visualized via Odyssey Infrared Fluorescent Western Blots Imaging System (Li-Cor Bioscience) or enhanced chemiluminescence (Cell Signaling Technology) and quantified via densitometry using Image J (version 1.42, National Institutes of Health).

Immunofluorescence

We used immunofluorescence to analysis the distribution of LC3B in hepatocytes, based on the protocol of Cai et al. [30]. In brief, after the indicated treatments, cells were washed in PBS and fixed in 4% paraformaldehyde at room temperature for 15 min. Then the cells were blocked for 1h in 5% BSA, and followed by incubation with specific primary antibodies rabbit anti-LC3B (1:500, ab51520; Abcam) overnight at 4 °C. The cells were washed thrice with PBS for 5 minutes each time, followed by incubation with a Goat Anti-Rabbit IgG H&L (Alexa Fluor® 647, 1:500, ab150079; Abcam) secondary antibody for 60 min at room temperature in the dark. DAPI was used to stain the nucleus of hepatocytes. The images were captured with the laser scanning confocal microscope (Leica) ($\times 40$ objective and $\times 5$ zoom, scale bar: 7.5 μ m), and fluorescence intensity was quantified by software Image J.

Dual luciferase reporter assay for detecting ChoRE at the PPAR γ promoter region

Based on the PPAR γ promoter characterized in our recent study [31], we constructed PPAR γ promoter into the pGL3 basic vector with ClonExpressTM II One Step Cloning Kit (Vazyme, Piscataway, NJ, USA). The carbohydrate response element-binding protein (ChREBP) binding sites [carbohydrate response element (ChoRE), 5'-GGCACGTGTG-3'] in the PPAR γ promoter from yellow catfish were predicted by JASPAR database (<http://jaspar.genereg.net/>). The site mutation of the ChoRE was performed with the Quick-Change Site-Directed Mutagenesis Kit

(Vazyme). These mutated constructs were named mutation 1 (5'-ATGCGCGCAT -3') and mutation 2 (5'-TAGGGCGCGA-3'). HEK 293T cells were transfected with different plasmids by using Lipofectamine 2000 Transfection Reagent (Thermo Fisher Scientific) in 24-well plates. Cells were collected to assay luciferase activity by the Dual-Luciferase Reporter Assay System (Promega, Minneapolis, MN, USA) according to the manufacturer's instructions.

EMSA (electrophoretic mobility shift assay) analysis for detecting the direct binding of ChoRE at the PPAR γ promoter

EMSA analysis for detecting the direct binding of ChoRE at the PPAR γ promoter followed the protocols described in our recent publications [31, 32]. Nuclear proteins were prepared and determined by the bicinchoninic acid method. Each oligonucleotide duplex of ChoRE (5'-AGTGTGGCACGTGTGTAATA-3') was incubated with 10 μ g nuclear extracts according to the manufacturer's instructions. The reaction mixture was incubated at room temperature for 30 min, and then detected by electrophoresis on 6% native polyacrylamide gels and ultimately transferred to a nylon membrane. The transferred DNA was cross-linked to the membrane and detected by chemiluminescence reaction. Competition analyses were performed by using 100-fold of unlabeled oligonucleotide duplex, with or without the mutation. These mutated constructs were named mutation 1 (5'-AGTGTATGCGCGCATTAATA-3') and mutation 2 (5'-AGTGTTAGGGCGCGATAATA-3').

Statistical analysis

Results were expressed as mean \pm S.E.M.. Firstly, the normality of the different treatments was evaluated with the Shapiro-Wilk test. Then, all data were evaluated by one-way analysis of variance and further analyzed by post hoc Duncan's multiple range testing to determine statistical significance. For the comparison between two groups, Student's *t* tests were used (unpaired, two-tailed). The analysis was performed with SPSS 19.0 (IBM, Armonk, NY, USA). *P* < 0.05 was considered significant.

Results

Growth performance, morphological parameters and serum glucose

In the present study, the survival was 100% among the three treatments (Supplementary Table 3). WG, SGR and FI (feed intake) increased with dietary carbohydrate levels. However, the FCR (feed conversion rate) declined with the

increase of dietary carbohydrate supplementation ($P < 0.05$). HSI tended to increase with dietary carbohydrate levels but the differences were not statistically significant among three treatments. VSI and VAI showed no significant differences among three treatments.

HCD increases liver lipid accumulation

The amount of cytoplasmic vacuolation in the liver was highest in HCD group than those in LCD and ICD groups (Supplementary Fig. 1A-C). HCD increased the amount of hepatic lipid droplets (Supplementary Fig. 1D-F) and hepatic TG content (Supplementary Fig. 1G). These observations were further confirmed by the areas quantified for lipid droplets in the H&E and Oil Red O staining (Supplementary Fig. 1H and I).

HCD increased lipogenesis and reduced lipolysis and fatty acid β -oxidation

Activities of lipogenic enzymes (G6PD, 6PGD and FAS) increased with dietary carbohydrate levels, but ICDH and ME activities showed no marked differences among the three treatments (Supplementary Fig. 2A). Glucose transporter 2 (GLUT2) is a high capacity transporter expressed in the livers [33]. The hepatic GLUT2 mRNA abundances for fish fed the HCD (Supplementary Fig. 2B) were higher than those in the LCD and ICD groups. The mRNA abundances of lipogenic genes (G6PD, FAS and ACCa), and the transcriptional factors related to lipogenesis (PPAR γ , SREBP-1, LXR α and ChREBP) for fish fed the HCD (Supplementary Fig. 2C) were higher than those in the LCD and ICD groups. 6PGD mRNA levels tended to increase with dietary carbohydrate levels. mRNA abundances of the lipolytic genes CPT1A and HSL for fish fed the HCD were lower than those in the LCD and ICD groups. The mRNA abundances of mitochondria (ACADL, ACAD8) and peroxisomal β -oxidation (ACAA2) for fish fed the HCD were lower than those in the LCD group, but the mRNA level of ACADVL, ACADSB, HADHAB, ECSH1, ACOX1 and ACAA1 showed no marked differences among the three treatments (Supplementary Fig. 2D).

HCD triggers hepatic ER stress, UPR and oxidative stress

To determine whether dietary carbohydrate cause ER stress, UPR and oxidative stress, thereby mediating the change of lipid metabolism, we first examined the ultrastructural changes of the liver. HCD caused the swelling of ER (Fig. 1A), indicating the occurrence of ER stress. Then, we examined if HCD influenced the mRNA expression of marker genes of ER stress and UPR (Fig. 1B). The mRNA expression of liver GRP78/BiP were significantly increased in HCD group, further

confirming HCD-induced occurrence of ER stress. The mRNA levels of hepatic PERK, eIF2 α and ATF6 were significantly higher in the HCD group than those in LCD and ICD groups, indicating the HCD-induced activation of PERK–eIF2 α and ATF6 pathways. Western blotting analysis indicated that the protein levels of ER stress markers (GRP78) were significantly higher in HCD group than those in ICD groups (Fig. 1C and D). SOD activities and the ratio of GSH/GSSG decreased with dietary carbohydrate levels (Fig. 1E and G), and that the MDA levels increased with dietary carbohydrate addition (Fig. 1F), indicating the activation of oxidative stress.

HCD increased hepatic autophagosome formation

Given the evidence that autophagy regulates lipid metabolism [6], we investigated the effect of HCD on autophagy. TEM observations demonstrated that HCD increased the number of LDs, which was accompanied by increased autophagosome formation (Fig. 2A–C). Some LDs were combined with the autolysosome, indicating a direct interaction between autophagy and lipid metabolism (autophagy-mediated lipophagy). The mRNA levels of autophagy-related genes (ATG1A, ATG6, ATG4A, ATG5, ATG7, ATG8A, ATG8B, ATG9A, ATG9B and p62) were significantly higher in HCD group than those in LCD group (Fig. 2D). Moreover, the protein levels of autophagy markers (LC3B-II and Beclin-1) were significantly higher in HCD group than those in LCD group (Fig. 2E and F). These results confirmed that HCD induced autophagy.

Lipophagy mediates high glucose (HG)-induced changes of lipid metabolism

To gain insight into the mechanisms of lipophagy mediating the high glucose-induced change in lipid metabolism, we isolated the primary hepatocytes from yellow catfish and conducted several *in vitro* experiments. The MTT assay showed that glucose concentrations of 5–25 mM had no significant influence on the viability of hepatocytes (Supplementary Fig. 3A). Thus, we choose the dose of 10mM glucose as HG (high glucose) group in the *in vitro* experiments and the concentration showed optimum response in TG accumulation and also is also a physiologically relevant dose in the plasma of yellow catfish fed the HCD. HG incubation increased GLUT2 mRNA expression and TG content (Supplementary Fig. 3B and C). HG also up-regulated mRNA expression of Plin2 and Plin3 (the LD-specific coat protein) (Supplementary Fig. 3D). Bodipy 493/503 staining further confirmed that HG incubation led to elevated LD accumulation (Supplementary Fig. 3E and F).

Then, we used seven methods to confirm the HG-induced autophagosome

formation. MDC is widely used as a probe to label autophagic vacuoles whereas Lyso-Tracker Red is used for labeling lysosomes specifically. Depending on the acidity of AO, autophagic lysosomes presented as orange/red fluorescent vesicles, whereas nuclei appeared green [28]. AO, MDC, and Lyso-Tracker Red staining demonstrated that HG incubation increase intracellular acidic compartments (Supplementary Fig. 4A-G). Co-staining with MDC and Lyso-Tracker Red demonstrated that HG increased autophagosomes (blue dots), autolysosomal (red dots) formation and autophagic flux (purple dots), indicating HG-induced increase of autophagic flux (Supplementary Fig. 4G). Meanwhile, TEM observation confirmed that the intracellular acidic vesicles correlated with the formation of autophagosomes and that HG incubation increased autophagosomes (Fig. 3A). Immunoblot analysis of Beclin-1 and LC3B-II (autophagosome marker), and p62/SQSTM1 (autophagic flux protein) revealed that HG up-regulated the protein expression of Beclin-1 and LC3B-II, and down-regulated P62 protein expression (Fig. 3B and C), indicating that HG increased autophagosome formation and autophagic flux. Besides, we used immunofluorescence to assess autophagosome marker LC3, and found HG-induced increase of fluorescence intensity (Fig. 3D and E). Overall, these data confirmed that HG increased autophagosome formation.

To detect the role autophagy plays in regulating HCD-induced changes of lipid deposition, we treated cells with two autophagy inhibitors which block autophagy via distinct mechanisms: 3-methyladenine (3-MA, suppressing the activity of class III PI3K) and CQ (inhibition of lysosome function). 3-MA or CQ incubation showed no significant effect on cell viability (Supplementary Fig. 5A), and intracellular TG contents (Supplementary Fig. 5B). However, 3-MA and CQ pre-treatment tended to increase the HG-induced TG deposition although the differences did not reach statistical significance in the CQ pre-treated group. Bodipy 493/503 staining confirmed that 3-MA and CQ pre-incubation increased green mean fluorescence intensity and the number and size of LDs induced by HG (Supplementary Fig. 5C and K). Meanwhile, we quantified autophagy by flow cytometric analysis of the red/green fluorescence ratio using AO staining. 3-MA or CQ pretreatment alleviated the HG-induced increase in the red: green fluorescence ratio (Supplementary Fig. 5F and G). Confocal microscopic images of hepatocytes stained with AO indicated that 3-MA or CQ pretreatment alleviated the HG-induced autophagy (Supplementary Fig. 5J). MDC staining showed that 3-MA pretreatment alleviated but CQ pretreatment

up-regulated the HG-induced increase in the fluorescence density (Supplementary Fig. 5D). This is understandable because 3-MA and CQ inhibited different processes of autophagy. 3-MA is an early-stage autophagy inhibitor and suppresses the activity of class III PI3K, and CQ is a late-stage autophagy inhibitor that blocks fusion of autophagosomes with lysosomes. Lyso-Tracker Red staining showed that 3-MA or CQ pretreatment alleviated the HG-induced increase in the fluorescence density (Supplementary Fig. 5E), and alleviated the HG-induced autophagy (Supplementary Fig. 5I). Taken together, all of these observations prove that autophagy mediated HG-induced changes of lipid deposition.

Lipophagy mediated HG-induced changes in lipid metabolism

To determine whether LDs are associated with lipophagy, we performed the co-localization studies of autophagosomes, lysosomes and LDs. The colocalization of the autolysosomes and the LDs was observed in hepatocytes co-stained with Lyso-Tracker Red (red) and Bodipy 493/503 (green). HG induced the increase of LDs' amounts and the colocalization of the autolysosomes (red) and the LDs (green), which indicated the induction of lipophagy (yellow) (Fig. 4A and B). TEM analysis confirmed that LDs integrated with the autolysosomes in HG-treated cells, indicating the occurrence of HG-induced lipophagy (Fig. 4C). To further confirm the role of lipophagy in HG-induced changes of lipid metabolism, we analyzed some parameters involved in lipid metabolism (Fig. 4D-G). HG induced the increases in intracellular NEFA content, indicating an increased flux in TG breakdown from LDs (Fig. 4E). HG incubation also up-regulated the mRNA levels of fatty acid binding protein liver-B, long-chain fatty acyl-CoA synthetases (ACSL1 and -4), acyl-CoA binding proteins (ACBP-4 and -5), consistent with enhanced NEFA release (Fig. 4D). However, HG treatment decreased CPT I activity (lipolytic enzyme) and mRNA expression of CPT1A, and increased the activities of 6PGD, G6PD, ME, and FAS (lipogenic enzymes) (Fig. 4D, F and G). These indicated that HG activated lipogenesis and inhibited lipolysis which in turn increased TG synthesis, consistent with increased flux in TG breakdown from LDs, indicating that lipophagy plays a regulatory role in the dynamic balance of lipogenesis and lipolysis.

Oxidative stress mediated HG-induced lipophagy and lipid accumulation

In an attempt to elucidate the mechanism of oxidative stress mediating HG-induced lipophagy and HG-induced changes of lipid metabolism, we used NAC (ROS scavenger) to block oxidative stress pathway. First, NAC did not significantly

influence the viability (Fig. 5A) of hepatocytes. NAC pre-treatment abrogated the HG-induced reduction in SOD activity and the ratio of GSH/GSSG, and HG-induced increase in MDA and ROS contents (Fig. 5B-E, and O). Also, NAC pretreatment alleviated the HG-induced increase in the contents of TG and NEFA, activities of lipogenic enzymes (G6PD, 6PGD, and FAS), and alleviated HG-induced reduction in CPT I activity (lipolytic enzyme) (Fig. 5F-M). Meantime, NAC pre-treatment alleviated the HG-induced increase in the mRNA expression of lipogenic genes and transcription factors (G6PD, 6PGD, ACCa, FAS, SREBP-1, PPAR γ , and ChREBP), and alleviated the HG-induced reduction in mRNA expression of lipolytic genes (LPL, and CPT1A) (Supplementary Fig. 6A). Furthermore, NAC pretreatment alleviated the HG-induced increase in the red: green fluorescence ratio (Fig. 5N and P) and in relative mRNA expression of autophagy related genes (Supplementary Fig. 6B). Overall, these data demonstrate that the oxidative stress played an important role in the HG-induced activation of lipophagy and HG-induced changes of lipid metabolism.

ER stress was involved in HG-induced lipophagy activation and lipid metabolism

Next, we explored the mechanism of ER stress mediating HG-induced changes of lipid metabolism and lipophagy. Firstly, TEM observation revealed that HG treatment induced swelling and altered morphology of ER (Fig. 6A). ER is the main depot for intracellular free Ca²⁺ and Ca²⁺ will be released from ER to cytoplasm when ER stress occurs. We found that HG treatment led to the time-dependent increase in Ca²⁺ fluxes (Fig. 6B and C), and up-regulated the protein expression of GRP78/Bip (ER stress marker protein) (Fig. 6D and E). These results confirmed that HG induced ER stress. As a chemical chaperone, 4-PBA was reported to alleviate ER stress [30]. We found that 4-PBA had no marked effect on cell viability (Fig. 6F). However, 4-PBA pretreatment significantly suppressed the HG-induced increase in mRNA expression of GRP78, PERK, eIF2 α , ATF4 and IRE1 α (Supplementary Fig. 7A). 4-PBA pretreatment reduced HG-induced increase of TG content although the differences were not statistically significant (Fig. 6G). Furthermore, 4-PBA pretreatment markedly abolished the HG-induced increase in activities of lipogenic enzymes (G6PD and FAS) (Fig. 6H-L), but had no significant effect on HG-induced reduction in CPT I activity (lipolytic enzyme) (Fig. 6M). 4-PBA pre-treatment also alleviated the HG-induced increase in mRNA expression of lipogenic genes and transcription factors (6PGD, ACCa, FAS, SREBP-1, PPAR γ , and ChREBP), and

1
2
3
4
5
6
7
8
9
10
11
12
13
14
15
16
17
18
19
20
21
22
23
24
25
26
27
28
29
30
31
32
33
34
35
36
37
38
39
40
41
42
43
44
45
46
47
48
49
50
51
52
53
54
55
56
57
58
59
60
61
62
63
64
65

477 HG-induced reduction in mRNA expression of lipolytic PPAR α (Supplementary Fig.
478 7B). In addition, 4-PBA pretreatment alleviated the HG-induced increase in the red:
479 green fluorescence ratio (Fig. 6N and O) and mRNA expression of autophagy related
480 genes (Supplementary Fig. 7C). Taken together, all these results support that ER stress
481 mediated HG-induced lipophagy activation and changes of lipid accumulation.

482 **HG triggers the activation of lipophagy and changes of lipid metabolism through** 483 **PPAR γ pathway**

484 To determine whether HG influenced mRNA expression of lipogenesis-related
485 transcription factors, the mRNA levels of PPAR γ , SREBP-1, PPAR α , and ChREBP
486 were measured (Supplementary Fig. 6A). PPAR γ was the key integrator of lipid
487 metabolism and autophagy [20, 34]. The present study indicated that HG significantly
488 up-regulated the mRNA and protein levels of PPAR γ (Fig. 7A-C). Next, we used
489 T0070907 (PPAR γ specific inhibitor) to explore the effects of PPAR γ signaling on
490 lipid metabolism and autophagy. As expected, T0070907 pretreatment abolished the
491 HG-induced TG accumulation (Fig. 7D) and alleviated HG-induced increase in the
492 mRNA levels of lipogenic genes (G6PD, 6PGD, ACC α , FAS, SREBP-1 and ChREBP)
493 (Supplementary Fig. 8A). T0070907 pretreatment also alleviated HG-induced
494 increase in mRNA expression of genes involved in autophagosome membrane
495 initiation (ATG1B and ATG6), autophagosome membrane expansion (ATG3, ATG4B
496 and ATG5), vesicle recycling (ATG13 and ATG9A) and cargo recruitment (ATG8B
497 and p62) (Supplementary Fig. 8B). Additionally, T0070907 pretreatment alleviated
498 HG-induced increase of the red: green fluorescence ratio (Fig. 7 E and F). All of these
499 results indicated that PPAR γ mediated HG-induced lipophagy activation and changes
500 of lipid metabolism.

501 In an attempt to elucidate the mechanisms of HG activating lipophagy- and lipid
502 metabolism- relevant genes at the transcriptional level, we further explored how HG
503 modulated PPAR γ signaling. ChREBP has emerged as a major mediator of
504 intracellular glucose-sensory transcriptional activator and regulates gene expression
505 by binding to the ChoRE motif of target genes [35]. By analyzing the promoter
506 regions of PPAR γ obtained in our laboratory [31], we found that ChoRE was located
507 at -534 to -515 bp of PPAR γ promoter region of yellow catfish, which consisted of the
508 evolutionarily conserved core sequence CACGTG (Fig. 7G). Thus, we used luciferase
509 reporter system to estimate whether HG could transcriptionally regulate the PPAR γ
510 promoter activity, and site-mutation analysis of ChREBP binding sites on

pGI3-PPAR γ -784/+63 vectors (mutations 1 and 2) was used to estimate the importance of the putative ChoRE sequences. Interestingly, our results revealed that HG incubation remarkably enhanced the luciferase activity of PPAR γ promoter (Fig. 7H), and the mutation of ChoRE significantly reduced the luciferase activity of the PPAR γ promoter. The mutation of site 1 (Mutation-1) did not significantly affect the HG-induced changes of the relative luciferase activity, but the mutation-2 at ChoRE binding site suppressed the HG-induced increase of luciferase activity, suggesting that ChREBP transactivated PPAR γ by binding to the ChoRE motif in the PPAR γ promoter region. Thus, the ChoRE motif was important for the HG-induced mRNA expression of PPAR γ . Next, we used EMSA assay to determine whether ChREBP can directly bind with the promoter region of PPAR γ . Our EMSA analysis indicated that the putative ChoRE sequences of the PPAR γ promoter could directly bind with nuclear extract; the direct interaction can be disrupted by unlabeled wild-type and restored by the mutant probes (Fig. 7I). Moreover, HG incubation can significantly enhance the binding activity of ChREBP to ChoRE (Fig. 7I, lane 6), suggesting that the -534 to -515 bp region of PPAR γ promoter could react with ChREBP. Together, these evidences confirmed that HG-activated lipophagy and lipid metabolism occurs via enhancing ChREBP DNA binding to the PPAR γ promoter region.

Discussion

In agreement with many other studies [35, 36], our study indicated that high dietary carbohydrate supplementation induced the lipid accumulation. Furthermore, our result indicated that HCD increased hepatic TG accumulation via the upregulation of lipogenesis and the downregulation of lipolysis. Similarly, Postic et al. [35] reported that a diet rich in carbohydrate stimulates lipogenic pathways. Here, increasing dietary carbohydrate levels also up-regulate dietary energy content, which in turn will increase lipid deposition and influence lipid metabolism, as reported in other studies [23,37].

Autophagy is important for regulating energy homeostasis and lipid content in hepatocytes [6]. The present study indicated that high carbohydrate induced autophagosome formation and that autophagy mediated HG-induced changes of lipid metabolism. Similarly, Gou et al. [38] showed that the expression of LC3B-II was markedly increased, and the autophagic vacuoles in cytoplasm was markedly accumulated when the HK2 cells were treated with high glucose. Emerging evidence indicates that LC3B-II, an autophagosome protein, is co-localized with lipid droplets;

lipid droplet-specific autophagy has since been termed lipophagy [6]. The present study found that HG incubation activated lipophagy and increased intracellular NEFA content, indicating an increased flux in TG breakdown from LDs. Thus, our study indicated that lipophagy regulated HG-induced changes in lipid metabolism.

In order to explore the mechanism of high carbohydrate addition inducing autophagy, we determine the HG-induced changes of oxidative and ER stress. Our data indicated that ROS and ER stress mediated the HG-induced autophagy. Similarly, Wang et al. [39] pointed out that ER stress triggered autophagy. Other studies pointed out that ER stress was involved in lipid accumulation [29, 40], which was also observed in the present study. Oxidative stress and ROS production together with ER stress caused lipid peroxidation and resulted in autophagy through several distinct mechanisms involving autophagy-related genes and antioxidant enzymes [11]. The decreased GSH/GSSG ratio and SOD activity were hallmarks of oxidative stress and is involved in autophagy [41, 42]. Chen et al. [41] indicated that increasing oxidative stress upregulated autophagy. Zhao et al. [43] pointed out that oxidative stress mediated fructose-induced TG deposition in BRL-3A cells. In the present study, pretreatment with antioxidant NAC impaired the reduction in GSH/GSSG ratio and SOD activity, and significantly abrogated ROS production, and in turn, prevented autophagy activation and lipid accumulation, suggesting the important role of oxidative stress in mediating HG-induced lipophagy and lipid metabolism.

Next, we further explored the direct relationship between HG-induced lipophagy activation and the HG-induced changes of lipid metabolism. Studies pointed out that PPAR γ was a key regulator of the transcriptional control of genes involved in lipid metabolism and autophagy [20, 34]. PPAR γ activation can induce autophagy and lipid accumulation [20, 44]. Our present study found that HG upregulated the mRNA and protein expression of PPAR γ ; Moreover, HG-activated lipophagy and lipid accumulation occurs via enhancing ChREBP DNA binding to the PPAR γ promoter region, which in turn induced transcriptional activation of the key autophagy- and lipogenesis-related genes [44, 45]. ChREBP is considered to be a pivotal sensor protein of intracellular glucose, specifically binding to the ChoRE promoter region of its downstream target genes [35]. Postic et al. [35] showed that ChREBP was required for the carbohydrate-induced transcriptional activation of enzymes involved in TG synthesis. Therefore, ChREBP has emerged as a major mediator of glucose action on lipogenic gene expression and appears to act as a central “bridge” which connected

the glucose and metabolic process. Here, we identified the putative ChoRE motif (5'-GGCACGTGTG-3') in the PPAR γ promoter region at -534 and -515 bp. Moreover, the dual luciferase reporter assay and EMSA assay revealed a direct link between ChREBP and PPAR γ , which indicated that endogenous ChREBP protein was recruited to the putative binding sites of PPAR γ .

Conclusion

Combining our data, we proposed a model, suggesting a novel mechanism of high carbohydrate diets inducing lipid accumulation (Supplementary Fig. 9). HCD induced lipogenesis and suppressed lipolysis, and activated lipophagy, oxidative and ER stress; lipophagy mediated HCD-induced changes of lipid metabolism via oxidative and ER stress pathways. Meanwhile, HG enhanced the ChREBP DNA binding capability at the ChoRE of PPAR γ promoter region, which in turn induced transcriptional activation of the key autophagy- and lipogenesis-related genes. It is noteworthy to point out that high dietary carbohydrate increased energy level, which potentially influences lipid metabolism and lipophagy. The mechanism of dietary energy levels influencing lipid metabolism and lipophagy remained to be investigated.

Acknowledgments

This work was supported by the National Key R&D Program of China (2018YFD0900400) and Fundamental Research Funds for the Central Universities, China (grant nos. 2662018PY089).

Disclosure of potential conflicts of interest

No potential conflicts of interest were disclosed.

Authors' contributions

Z.L. and T.Z. designed the experiments. T.Z. carried out animal and cell experiments and sample analysis with the help of K.W., Y.H.X., G.H.C., and C.C.W.; T.Z., Z.L. and C.H. analyzed data; T.Z. wrote the manuscript, and Z.L. and C.H. revised the manuscript. All the authors read and approved the manuscript.

References

1. Fabbrini E, Sullivan S, Klein S (2010) Obesity and nonalcoholic fatty liver disease: biochemical, metabolic, and clinical implications. *Hepatology* 51:679–689
2. Farrell GC, Larter CZ (2006) Non-alcoholic fatty liver: from steatosis to cirrhosis. *Hepatology* 43:S99–S112
3. Abdelmalek MF, Suzuki A, Guy C, Unalp-Arida A, Colvin R, Johnson RJ, Diehl AM (2010) Increased fructose consumption is associated with fibrosis severity in patients with nonalcoholic fatty liver disease. *Hepatology* 51:1961-1971

- 615 4. Neuschwander-Tetri BA (2013) Carbohydrate intake and nonalcoholic fatty liver
616 disease. *Curr Opin Clin Nutr* 16:446-452
- 617 5. Levine B, Klionsky DJ (2004) Development by self-digestion: molecular
618 mechanisms and biological functions of autophagy. *Dev Cell* 6:463-477
- 619 6. Singh R, Kaushik S, Wang YJ, Xiang YQ, Novak I, Komatsu M, Tanaka K,
620 Cuervo AM, Czaja MJ (2009) Autophagy regulates lipid metabolism. *Nature*
621 458:1131-1135
- 622 7. Bechmann LP, Hannivoort RA, Gerken G, Hotamisligil GS, Trauner M, Canbay A
623 (2012) The interaction of hepatic lipid and glucose metabolism in liver diseases. *J*
624 *Hepatol* 56:952-964
- 625 8. Dong HQ, Czaja MJ (2011) Regulation of lipid droplets by autophagy. *Trends*
626 *Endocrinol Metab* 22:234-240
- 627 9. Singh R, Cuervo AM (2012) Lipophagy: connecting autophagy and lipid
628 metabolism. *Int J Cell Biol* 2012:282041
- 629 10. Lavallard VJ, Gual P (2014) Autophagy and non-alcoholic fatty liver disease.
630 *Biomed Res Int* 2014:120179
- 631 11. Azad MB, Chen YQ, Gibson SB (2009) Regulation of autophagy by reactive
632 oxygen species (ROS): implications for cancer progression and treatment.
633 *Antioxid Redox Signal* 11:777-790
- 634 12. Kawai D, Takaki A, Nakatsuka A, Wada J, Tamaki N, Yasunaka T, Koike K,
635 Tsuzaki R, Matsumoto K, Miyake Y, et al (2012) Hydrogen- rich water prevents
636 progression of nonalcoholic steatohepatitis and accompanying
637 hepatocarcinogenesis in mice. *Hepatology* 56:912-921
- 638 13. Panieri E, Santoro MM (2016) ROS homeostasis and metabolism: a dangerous
639 liason in cancer cells. *Cell Death Dis* 7:e2253
- 640 14. Pan YX, Luo Z, Zhuo MQ, Wei CC, Chen GH, Song YF (2018) Oxidative stress
641 and mitochondrial dysfunction mediated Cd-induced hepatic lipid accumulation
642 in zebrafish *Danio rerio*. *Aquat Toxicol* 199:12-20
- 643 15. Wang H, Sun RQ, Zeng XY, Zhou X, Li SP, Jo E, Molero JC, Ye JM (2015)
644 Restoration of autophagy alleviates hepatic ER stress and impaired insulin
645 signalling transduction in high fructose-fed male mice. *Endocrinology*
646 156:169-181
- 647 16. Madaro L, Marrocco V, Carnio S, Sandri M, Bouché M (2013) Intracellular
648 signaling in ER stress-induced autophagy in skeletal muscle cells. *FASEB J*
649 27:1990-2000
- 650 17. Rutkowski DT, Wu J, Back SH, Callaghan MU, Ferris SP, Iqbal J, Clark R, Miao
651 H, Hassler JR, Fornek J, et al (2008) UPR pathways combine to prevent hepatic
652 steatosis caused by ER stress-mediated suppression of transcriptional master
653 regulators. *Dev Cell* 15:829-840
- 654 18. Werstuck GH, Lentz SR, Dayal S, Hossain GS, Sood SK, Shi YY, Zhou J, Maeda
655 N, Krisans SK, Malinow MR, et al (2001) Homocysteine-induced endoplasmic
656 reticulum stress causes dysregulation of the cholesterol and triglyceride
657 biosynthetic pathways. *J Clin Invest* 107:1263-1273
- 658 19. Patel L, Pass I, Coxon P, Downes CP, Smith SA, Macphée CH (2001) Tumor
659 suppressor and anti-inflammatory actions of PPAR γ agonists are mediated via
660 upregulation of PTEN. *Curr Biol* 11:764-768
- 661 20. Zheng JL, Zhuo MQ, Luo Z, Pan YX, Song YF, Huang C, Zhu QL, Hu W, Chen Q
662 L (2015) Peroxisome proliferator-activated receptor gamma (PPAR γ) in yellow
663 catfish *Pelteobagrus fulvidraco*: molecular characterization, mRNA expression
664 and transcriptional regulation by insulin *in vivo* and *in vitro*. *Gen Comp Endocr*

- 212:51-62
21. Meyer A, Van de Peer Y (2005) From 2R to 3R: evidence for a fish-specific genome duplication (FSGD). *Bioessays* 27:937–45.
22. Gong G, Dan C, Xiao S, Guo W, Huang P, Xiong Y, Wu J, He Y, Zhang J, Li X, et al (2018) Chromosomal-level assembly of yellow catfish genome using third-generation DNA sequencing and Hi-C analysis. *GigaScience* 7 doi: 10.1093/gigascience/giy120.
23. Ye WJ, Tan XY, Chen YD, Luo Z (2009) Effects of dietary protein to carbohydrate ratios on growth and body composition of juvenile yellow catfish, *Pelteobagrus fulvidraco* (Siluriformes, Bagridae, *Pelteobagrus*). *Aquac Res* 40:1410-1418
24. Wei CC, Luo Z, Hogstrand C, Xu YH, Wu LX, Chen GH, Pan YX, Song YF (2018) Zinc reduces hepatic lipid deposition and activates lipophagy via Zn^{2+} /MTF-1/PPAR α and Ca^{2+} /CaMKK β /AMPK pathways. *FASEB J* 32: 6666-6680
25. Yang SB, Tan XY, Zhang DG, Cheng J, Luo Z (2018) Identification of ten SUMOylation-related genes from yellow catfish *Pelteobagrus fulvidraco*, and their transcriptional responses to carbohydrate addition *in vivo* and *in vitro*. *Front Physiol* 9:1544
26. Wu K, Luo Z, Hogstrand C, Chen GH, Wei CC, Li DD (2018) Zn stimulates the phospholipids biosynthesis via the pathways of oxidative and endoplasmic reticulum stress in the intestine of freshwater teleost yellow catfish. *Environ Sci Technol* 52:9206-9214
27. Giustarini D, Dalle-donne I, Milzani A, Fanti P, Rossi R (2013) Analysis of GSH and GSSG after derivatization with n-ethylmaleimide. *Nat Protoc* 8:1660-1669
28. Klionsky DJ, Abdelmohsen K, Abe A, Abedin MJ, Abeliovich H, Arozena AA, Adachi H, Adams CM, Adams PD, Adeli K, et al (2016) Guidelines for the use and interpretation of assays for monitoring autophagy (3rd edition). *Autophagy* 12: 1-222
29. Song YF, Luo Z, Zhang LH, Hogstrand C, Pan YX (2016) Endoplasmic reticulum stress and disturbed calcium homeostasis are involved in copper-induced alteration in hepatic lipid metabolism in yellow catfish *Pelteobagrus fulvidraco*. *Chemosphere* 144:2443-2453
30. Cai XY, Liu YL, Hu YQ, Liu XZ, Jiang HY, Yang SH, Shao Z, Xia Y, Xiong L (2018) Ros-mediated lysosomal membrane permeabilization is involved in bupivacaine-induced death of rabbit intervertebral disc cells. *Redox Biol* 18:65-76
31. Wu K, Tan XY, Xu YH, Chen GH, Zhuo MQ (2018) Functional analysis of promoters of genes in lipid metabolism and their transcriptional response to STAT3 under leptin signals. *Genes* 9:334
32. Xu YH, Luo Z, Wu K, Fan YF, You WJ, Zhang LH (2017) Structure and functional analysis of promoters from two liver isoforms of CPT I in grass carp *Ctenopharyngodon idella*. *Int J Mol Sci* 18:E2405
33. Thorens B (1996) Glucose transporters in the regulation of intestinal, renal, and liver glucose fluxes. *Am J Physiol* 270:G541-G553
34. Assumpção JAF, Magalhães KG, Corrêa JR (2017) The role of ppar γ and autophagy in ros production, lipid droplets biogenesis and its involvement with colorectal cancer cells modulation. *Cancer Cell Int* 17:82.
35. Postic C, Dentin R, Denechaud PD, Girard J (2007) ChREBP, a transcriptional regulator of glucose and lipid metabolism. *Annu Rev Nutr* 27:179-192
36. Chen B, Zheng YM, Zhang JP (2018) Comparative study of different

- diets-induced NAFLD models of zebrafish. *Front Endocrinol* 9:366
37. Dias J, Alvarez MJ, Diez A, Arzel J, Corraze G, Bautista JM, Kaushik SJ (1998) Regulation of hepatic lipogenesis by dietary protein/energy in juvenile European sea bass (*Dicentrarchus labrax*). *Aquaculture* 161: 169-186.
 38. Gou R, Chen JT, Sheng SF, Wang RQ, Fang YD, Yang ZJ, Wang L, Tang L (2016) Kim-1 mediates high glucose-induced autophagy and apoptosis in renal tubular epithelial cells. *Cell Physiol Biochem* 38:2479-2488
 39. Wang H, Sun RQ, Camera D, Zeng XY, Jo E, Chan SM, Herbert TP, Molero JC, Ye JM (2016) Endoplasmic reticulum stress up-regulates Nedd4-2 to induce autophagy. *FASEB J* 30:2549-2556
 40. Lebeaupin C, Vallée D, Hazari Y, Hetz C, Chevet E, Bailly-Maitre B (2018) Endoplasmic reticulum stress signaling and the pathogenesis of non-alcoholic fatty liver disease. *J Hepatol* 69:927-947
 41. Chen Y, Azad MB, Gibson SB (2009) Superoxide is the major reactive oxygen species regulating autophagy. *Cell Death Differ* 16:1040-1052
 42. Zhang Z, Guo M, Zhao S, Shao J, Zheng S (2016) ROS-JNK1/2-dependent activation of autophagy is required for the induction of anti-inflammatory effect of dihydroartemisinin in liver fibrosis. *Free Radic Biol Med* 101:272-283
 43. Zhao, XJ, Yu, HW, Yang, YZ, Wu, WY, Chen, TY, Jia, KK, Kang, LL, Jiao, RQ, Kong, LD (2018) Polydatin prevents fructose-induced liver inflammation and lipid deposition through increasing miR-200a to regulate Keap1/Nrf2 pathway. *Redox Biol* 18:124-137
 44. Rovito D, Giordano C, Vizza D, Plastina P, Barone I, Casaburi I, Lanzino M, De A F, Sisci D, Mauro L, et al (2013) Omega-3 PUFA ethanolamides DHEA and EPA induce autophagy through PPAR γ activation in MCF-7 breast cancer cells. *J Cell Physiol* 228:1314-1322
 45. Zhou J, Zhang W, Liang B, Casimiro MC, Whitaker-Menezes D, Wang M, Lisanti MP, Lanza-Jacoby S, Pestell RG, Wang C (2009) PPAR γ activation induces autophagy in breast cancer cells. *Int J Biochem Cell Biol* 41:2334-2342

Figure captions:

Fig. 1 Dietary carbohydrate supplementation triggers ER stress, UPR and oxidative stress in the liver of yellow catfish. (A) Liver ultrastructure (TEM, original magnification $\times 10000$, bars, 1 μm). m, mitochondria; nu, hepatocyte nucleus; er, endoplasmic reticulum; sm, swelling and vesiculation of mitochondria; ser, swelling of endoplasmic reticulum. (B) The relative mRNA expression of genes involved in ER stress and UPR. (C) Western blot analysis of ER stress marker GRP78. (D) Relative quantification of protein levels of GRP78 were normalized to GAPDH. (E) Hepatic SOD activity. (F) Hepatic MDA content. (G) The ratio of GSH/GSSG in the liver. Values are mean \pm S.E.M. ($n = 3$ replicate tanks and was used as three biological replicates. At least three fish were sampled for each tank and used as technical replicates). mRNA expression values were normalized to housekeeping genes (β -actin and HPRT) expressed as a ratio of the LCD. P value was calculated by one-way ANOVA and further post hoc Duncan's multiple range testing. Values without the same letter indicate significant difference among three treatments ($P < 0.05$).

Fig. 2 Dietary carbohydrate supplementation increases hepatic autophagosome formation of yellow catfish. (A-C) Representative image of liver ultrastructure (TEM, Scale bars, 2 μm). Black arrows represent the autophagosome. (D) Relative mRNA levels of key hepatic autophagy-related genes. (E) Western blot analysis of LC3B and Beclin1. (F) Relative quantification of protein levels of LCB were normalized to β -actin and Beclin1 were normalized to GAPDH. Relative mRNA expression values were normalized to housekeeping genes (β -actin and HPRT) expressed as a ratio of the low carbohydrate diet LCD. All data are expressed as mean \pm S.E.M. ($n = 3$ replicate tanks and was used as three biological replicates. At least three fish were sampled for each tank and used as technical replicates). P value was calculated by one-way ANOVA and further post hoc Duncan's multiple range testing. Values without the same letter indicate significant difference among three treatments ($P < 0.05$).

Fig. 3 High glucose concentration activates autophagy of hepatocytes from yellow catfish. The primary hepatocytes from *P. fulvidraco* were incubated in control (5 mM glucose) or HG (10mM glucose) for 48 h in M199 medium. (A) Representative transmission electron microscope image of hepatocytes. Black arrows represent the autophagosome. (B and C) Western blot analysis of LC3B, Beclin1, and P62 protein levels ($n = 3$). (D and E) Representative confocal images and relative red fluorescence

intensity showing LC3-II protein by immunofluorescence staining. Relative protein levels of LC3B, Beclin1, and P62 were normalized to GAPDH. All data are expressed as mean \pm S.E.M. (n=3 at least). *P* value was calculated by Student's *t* tests. **P* < 0.05, ***P* < 0.01, compared with control.

Fig. 4 Lipophagy, which provided free fatty acids for the synthesis of TG but not for mitochondrial β -oxidation, alleviated HG-induced steatosis. The primary hepatocytes from *P. fulvidraco* were incubated in control (5 mM glucose) or HG (10mM glucose) for 48 h in M199 medium. (A) The co-localization of the autolysosomes and the lipid droplets in hepatocytes co-stained with 50nM Lyso-Tracker Red and 5 μ g/ml BODIPY 493/503 (green) indicating the induction of lipophagy (yellow). (B) Schematic representation of the colocalization between autolysosome and LDs; (C) Representative TEM image of hepatocytes after control or HG incubation. Black arrows represent the lipophagy; (D) The mRNA levels of genes in the hepatocytes related to the fatty acid metabolism and mitochondria β -oxidation. (E) NEFA content in hepatocytes; (F, G) Activities of lipogenic (6PGD, G6PD, ICDH, ME and FAS) and lipolytic (CPTI) enzymes in the hepatocytes. Relative mRNA expression values were normalized to housekeeping genes (EIFA and RPL7) expressed as a ratio of the control. All data are expressed as mean \pm S.E.M. (n=3 at least). *P* value was calculated by Student's *t* tests. **P* < 0.05, ***P* < 0.01, compared with control.

Fig. 5 Mitochondrial oxidative stress pathway mediated HG-induced autophagy and lipid accumulation in the primary hepatocytes of yellow catfish. The primary hepatocytes from *P. fulvidraco* were incubated in control (5mM glucose) or HG (10mM glucose) for 48 h in M199 medium with or without 2-h pretreatment with a ROS scavenger (0.5mM NAC). (A) Cell viability. (B-D) Activity of T-SOD, MDA content, and ratio of GSH/GSSG. (E) The intracellular ROS was quantified by calculating FL1 (green) mean fluorescence intensity (DCFH-DA fluorescent staining). (F-K) Activities of lipogenic (6PGD, G6PD, ICDH, ME and FAS) and lipolytic (CPTI) enzymes. (L) TG content. (M) NEFA content. (N) The autophagy was quantified by flow cytometric analysis of red/green (FL2/FL1) fluorescence ratio (acridine orange fluorescent staining, 1 μ M). (O) The presence of DCFH-DA-stained intracellular ROS was determined by flow cytometry analysis of green fluorescence intensity. (P) The presence of acridine orange-stained intracellular autophagic vacuole was determined by flow cytometry analysis of red/green (FL2/FL1) fluorescence ratio. All data are expressed as mean \pm S.E.M. (n=3 at least). *P* value was calculated by Student's *t* tests.

* $P < 0.05$, ** $P < 0.01$, compared with control; # $P < 0.05$, ## $P < 0.01$, compared with HG group.

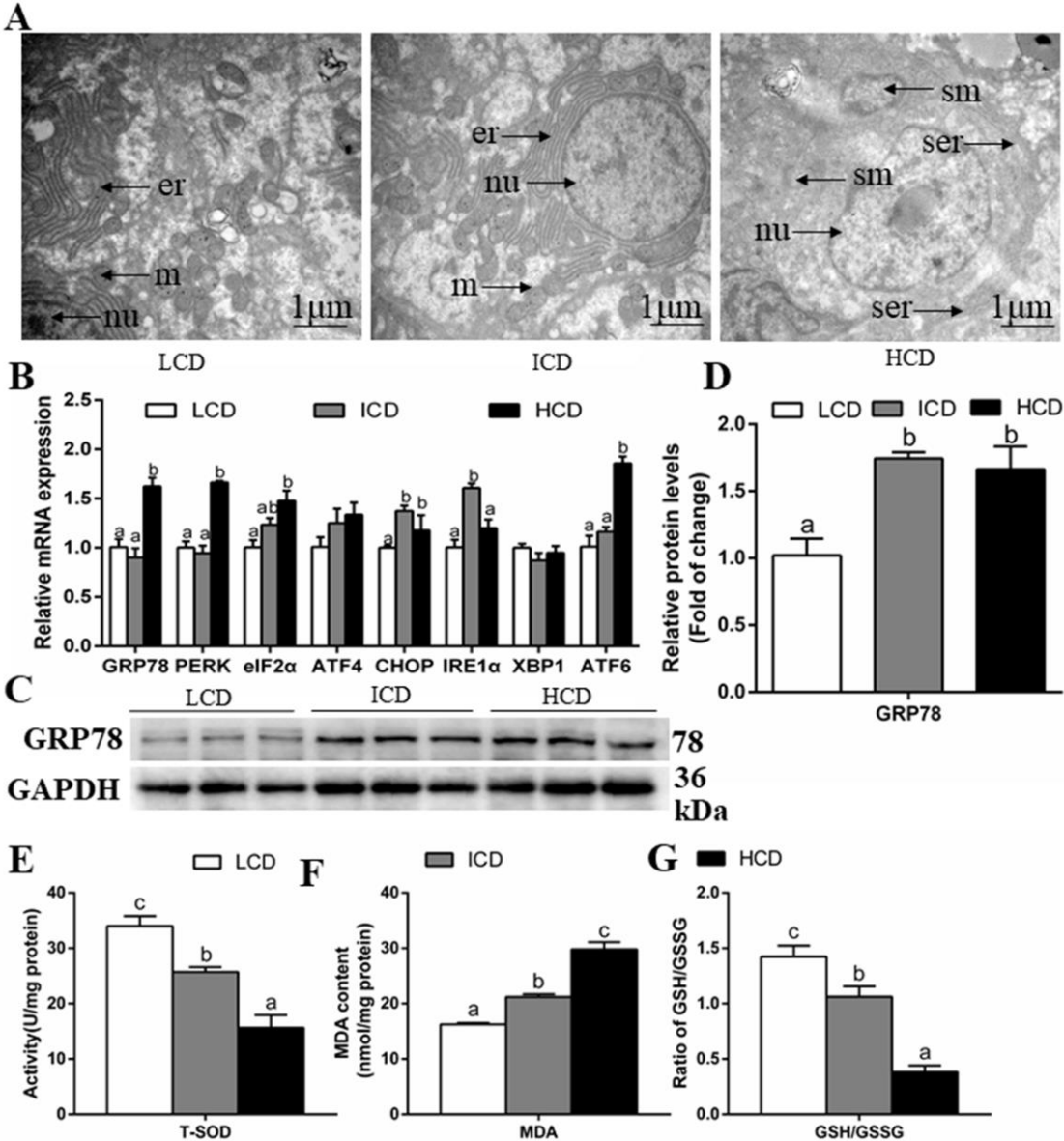
Fig. 6 ER stress pathway mediated HG-induced lipid deposition and autophagy of the primary hepatocytes from yellow catfish. Hepatocytes were incubated in control (5mM glucose) or HG (10mM glucose) for 48 h in M199 medium with or without 2-h pretreatment with an ER stress inhibitor (100 μ M 4-PBA). (A) Representative TEM images. Black arrow pointing to endoplasmic reticulum. (B) Representative confocal microscopy image of hepatocytes stained with Ca^{2+} fluorescent probe (Fluo-4 AM, 4 μ M), showing a time-dependent changes in green fluorescence levels of primary hepatocytes. (C) Schematic represent quantification of the Fluo-4 AM staining. (D, E) Western blot analysis of GRP78/Bip protein levels (n=3). (F) Cell viability. (G) TG content. (H-M) Activities of lipogenic (6PGD, G6PD, ICDH, ME and FAS) and lipolytic (CPTI) enzymes. (N) The autophagy was quantified by flow cytometric analysis of red/green (FL2/FL1) fluorescence ratio (acridine orange fluorescent staining, 1 μ M). (O) The presence of acridine orange-stained intracellular autophagic vacuole was determined by flow cytometry analysis of red/green (FL2/FL1) fluorescence ratio. All data are expressed as mean \pm S.E.M. (n=3 at least). P value was calculated by Student's t tests. * $P < 0.05$, ** $P < 0.01$, compared with control; # $P < 0.05$, ## $P < 0.01$, ### $P < 0.001$, compared with HG group.

Fig. 7 HG activates autophagy and lipid accumulation through PPAR γ pathway in hepatocytes of yellow catfish. (A) The mRNA levels of PPAR γ . (B, C) Western blot analysis of PPAR γ protein levels. (D) TG content of the primary hepatocytes from *P. fulvidraco* were incubated in control (5mM glucose) or HG (10mM glucose) for 48 h in M199 medium with or without 2-h pretreatment with 1 μ M T0070907 (PPAR γ inhibitor). (E) The autophagy was quantified by flow cytometric analysis of red/green (FL2/FL1) fluorescence ratio using 1 μ M acridine orange fluorescent staining. (F) The presence of acridine orange-stained intracellular autophagic vacuole was demonstrated by flow cytometry analysis of red-to-green (FL2/FL1) fluorescence ratio. (G) ChREBP binding sequence (ChoRE) located at -534 bp to -515 bp of PPAR γ promoter region of yellow catfish. (H) Site-mutation analysis of ChREBP binding sites on pGl3-PPAR γ -784/+63 vectors. (I) EMSA of putative PPAR γ binding sequences (ChoRE). The 5'-biotin labeled double-stranded oligomers were incubated with nuclear protein. A 100-fold excess of the competitor and mutative competitor oligomers was added to the competition and mutant competition assay, respectively. All data were expressed as mean \pm S.E.M. (n=3 at least). P value was calculated by Student's t tests. * $P < 0.05$, ** $P < 0.01$, compared with control; # $P < 0.05$, ## $P < 0.01$,

compared with HG group. The comparison between other groups was shown in the figure.

898

Figure 1

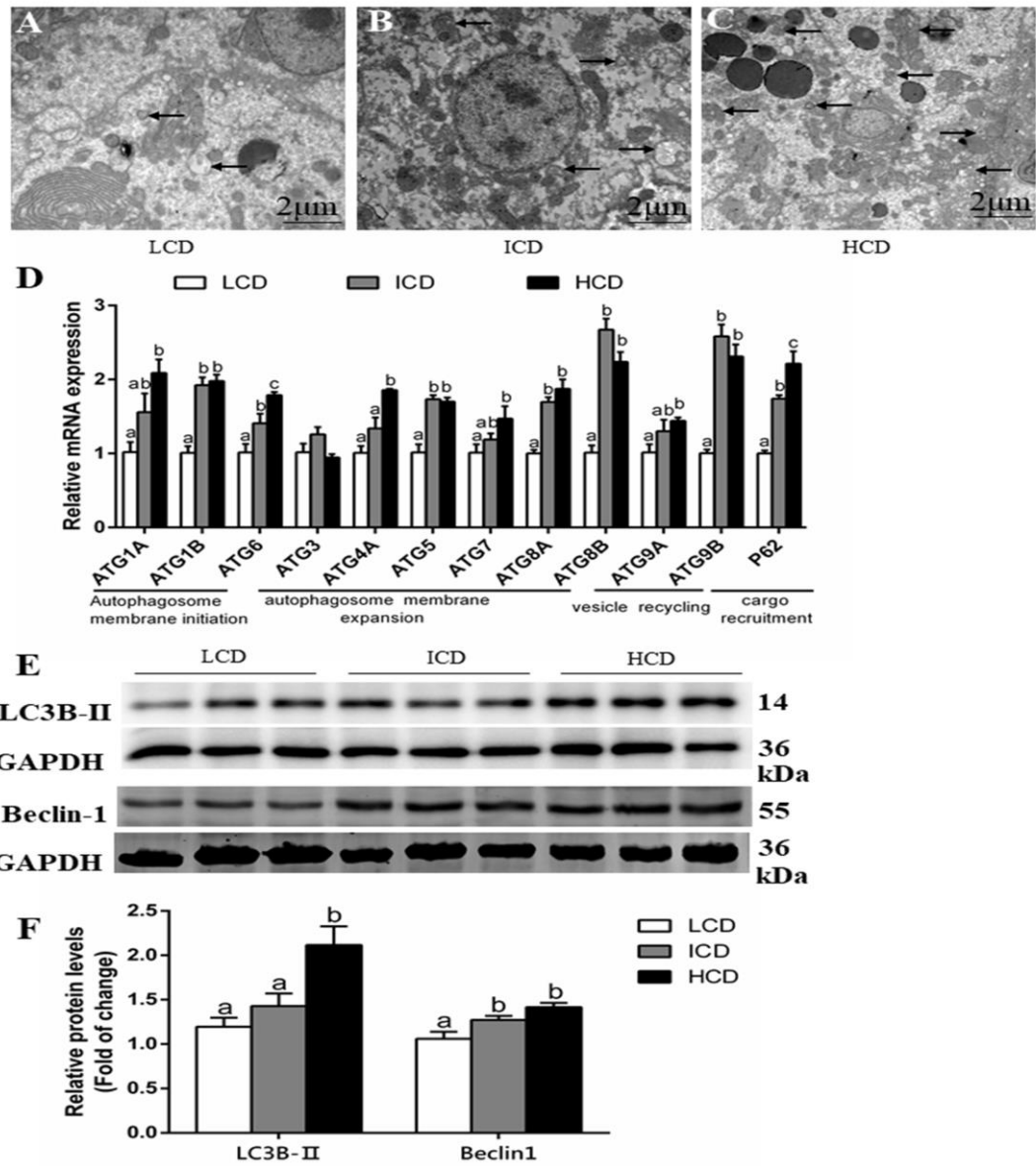


899

900

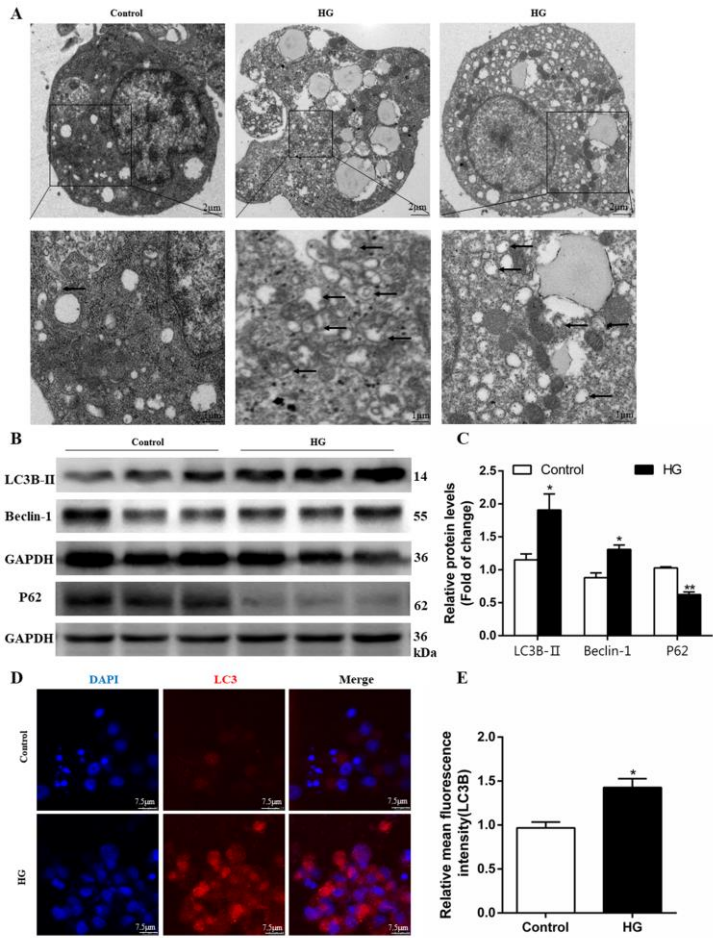
901

Figure 2



902

903 **Figure 3**
904



905

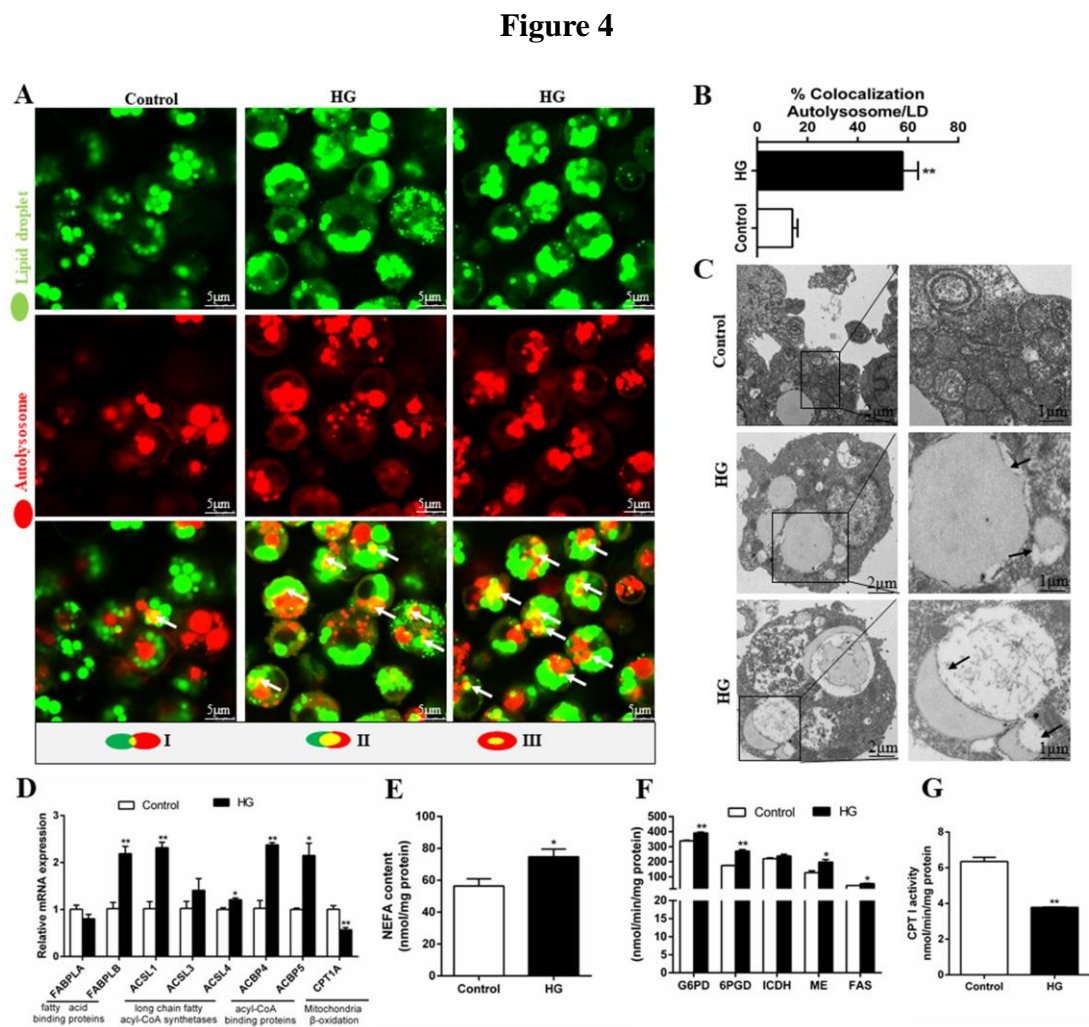


Figure 5

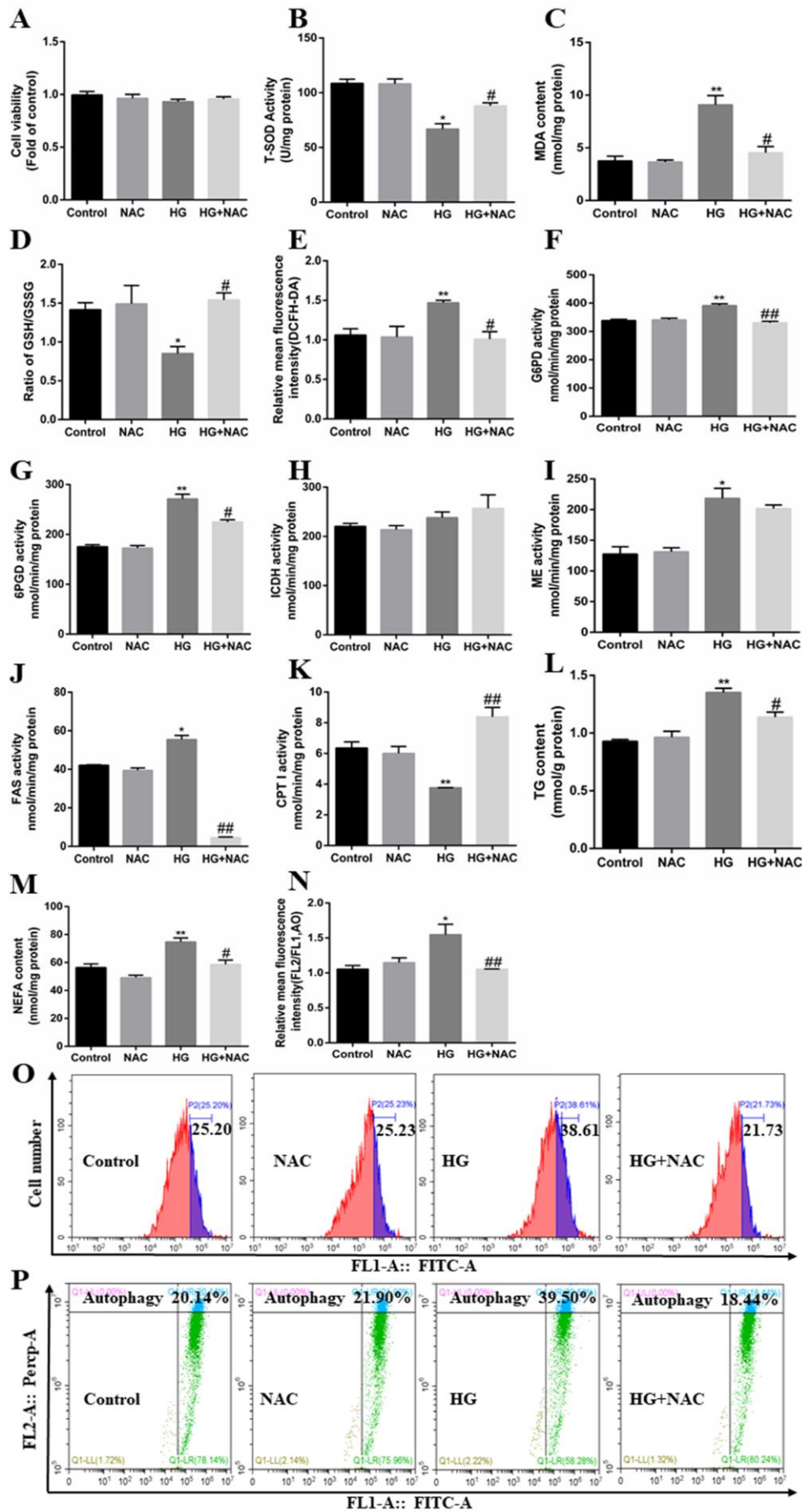
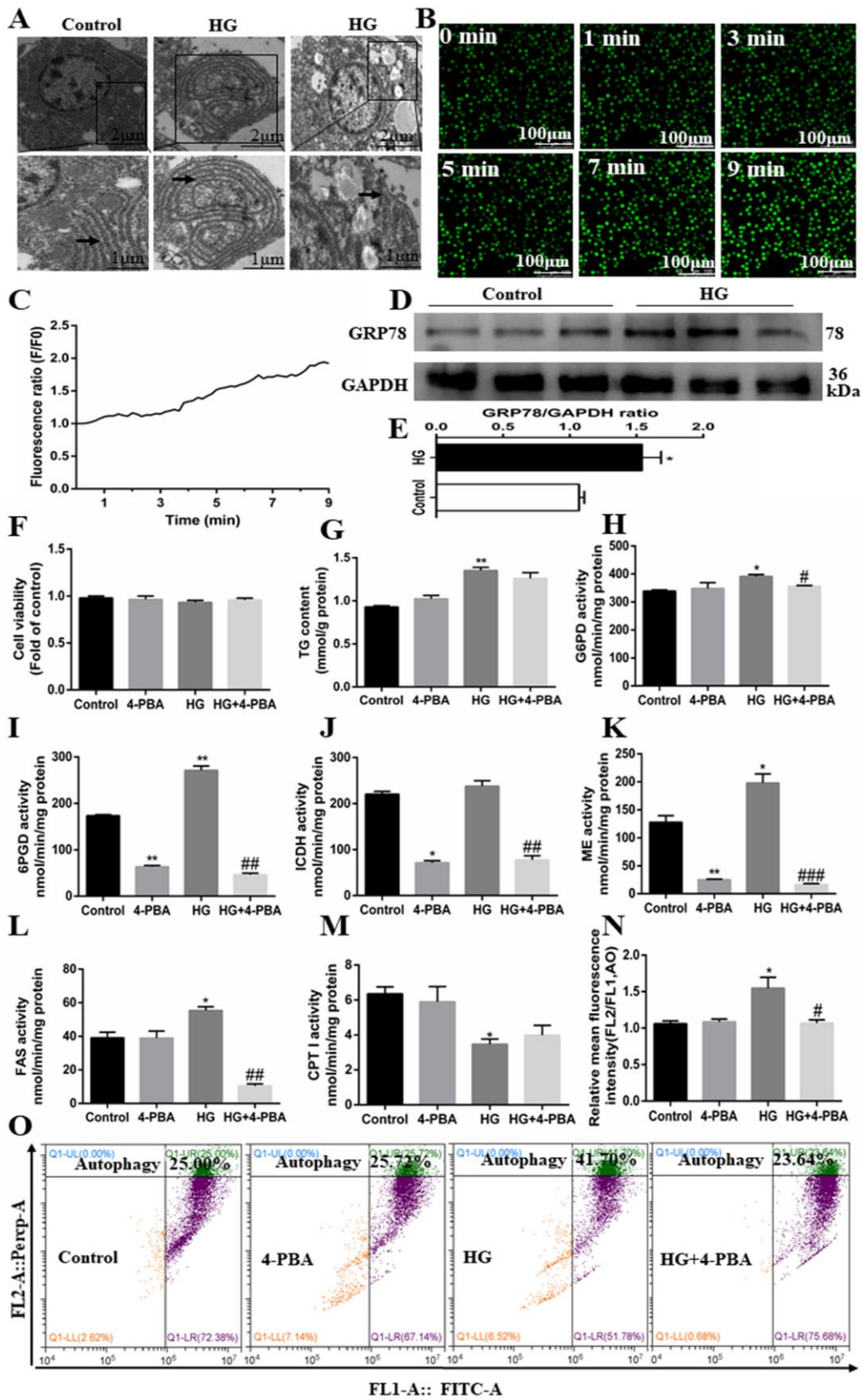
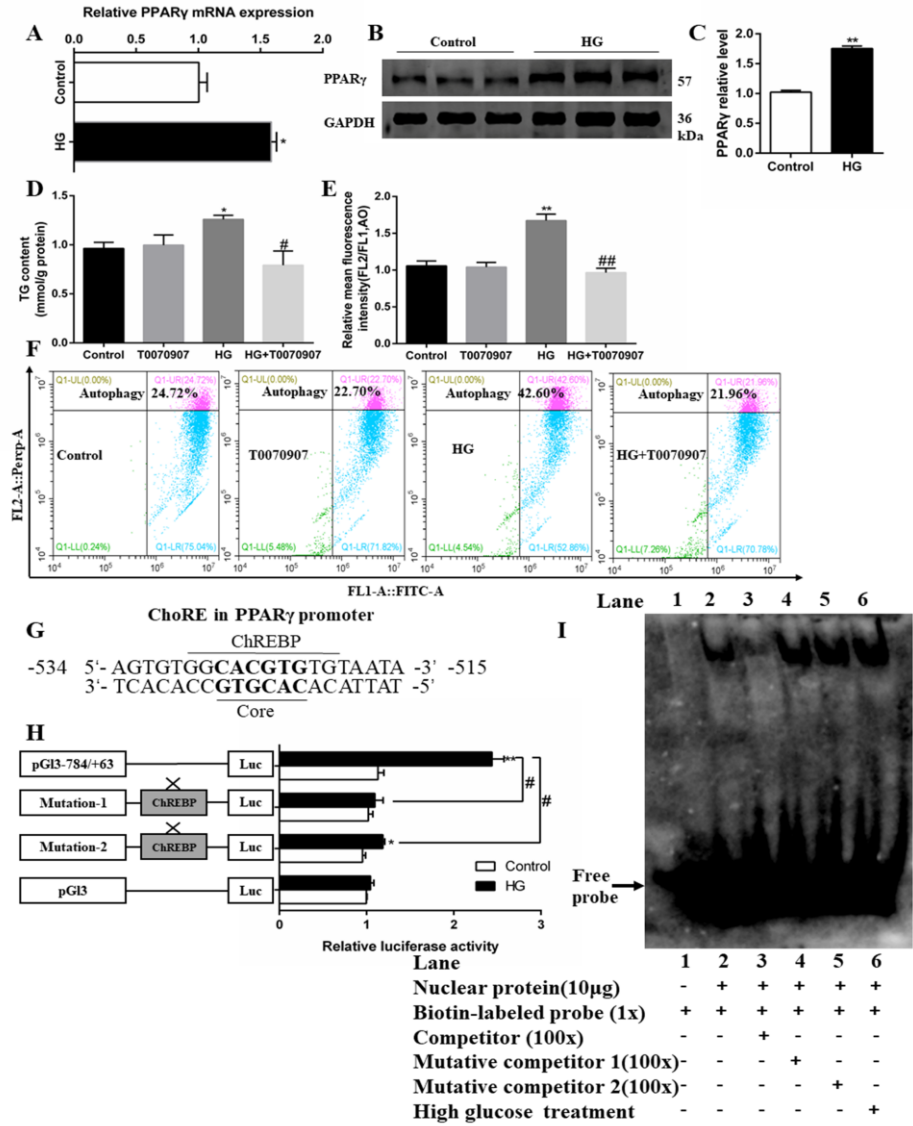


Figure 6



916

Figure 7



917



[Click here to access/download](#)

Supplementary Material

Supplementary materials20190705.doc

